Check for updates

2D noble metals: growth peculiarities and prospects for hydrogen evolution reaction catalysis

Ivan Shtepliuk [iD]

High-performance electrocatalysts for the hydrogen evolution reaction are of interest in the development of next-generation sustainable hydrogen production systems. Although expensive platinum-group metals have been recognized as the most effective HER catalysts, there is an ongoing requirement for the discovery of cost-effective electrode materials. This paper reveals the prospects of two-dimensional (2D) noble metals, possessing a large surface area and a high density of active sites available for hydrogen proton adsorption, as promising catalytic materials for water splitting. An overview of the synthesis techniques is given. The advantages of wet chemistry approaches for the growth of 2D metals over deposition techniques show the potential for kinetic control that is required as a precondition to prevent isotropic growth. An uncontrolled presence of surfactant-related chemicals on a 2D metal surface is however the main disadvantage of kinetically controlled growth methods, which stimulates the development of surfactant-free synthesis approaches, especially template-assisted 2D metal growth on non-metallic substrates. Recent advances in the growth of 2D metals using a graphenized SiC platform are discussed. The existing works in the field of practical application of 2D noble metals for hydrogen evolution reaction are analyzed. This paper shows the technological viability of the "2D noble metals" concept for designing electrochemical electrodes and their implementation into future hydrogen production systems, thereby providing an inspirational background for further experimental and theoretical studies.

1. Advantages of 2D noble metals

In the long-term, hydrogen technologies are foreseen to be the cornerstones of sustainable and renewable energy sources,[1,2] and will replace traditional fossil fuels.[3] With this target in mind, it is imperative to pay special attention to the implementation of new strategies of green hydrogen production and the improvement of existing technologies towards new hydrogen storage materials[4,5] and highly efficient catalysts for the hydrogen evolution reaction (HER).[6–10] The HER is a fundamentally important process in electrochemical water splitting for clean hydrogen production.[11–13] Even though platinum group metals (PGMs) are considered to be superior catalysts for the HER,[14,15] they are referred to as critical raw materials due to their limited abundance.[16] Indeed, the natural scarcity of noble metals (NMs) largely determines their high cost. Efficient catalysts should contain a high NM content to ensure a good performance, which impedes their large-scale production and implementation. More

efficient approaches should therefore be applied to ensure a scalable cost-efficient production of HER catalysts beyond the conventional bulk PGM-based ones. One of the possible solutions to address this challenge involves replacing PGM.[17–19] In this context, advanced non-PGM catalysts with a large surface area, high electrical conductivity, low toxicity, and appropriate catalytic activity (*i.e.*, near-to-zero Gibbs free energy of hydrogen adsorption (ΔG_{H^*}), as low as possible water decomposition barrier, wide potential window, fast charge transfer, and good stability, are highly sought. Despite huge efforts dedicated to developing advanced non-PGM catalytic materials,[20–22] parameters describing their catalytic activity in the HER are, in most cases, noticeably lagging behind the indicators of NM-based catalysts. PGMs are still the gold standard for the hydrogen evolution reaction. For this reason, even the lower cost of non-PGM materials does not play a decisive role. With an appropriate strategy, catalysts based on precious metals can be, however, re-designed and re-engineered towards less NM consumption and more cost-efficient technologies. This implies designing HER catalysts with as low a NM content as possible. To some extent, this can be achieved *via* a 3D-to-2D phase transformation. The main goal is to create planar (2D) arrays of metal atoms with low

Semiconductor Materials Division, Department of Physics, Chemistry and Biology-IFM, Linköping University, S-58183 Linköping, Sweden.
E-mail: ivan.shtepliuk@liu.se

This journal is © the Owner Societies 2023

Phys. Chem. Chem. Phys., 2023, **25**, 8281–8292 | 8281

coordination numbers that will eventually lead to the discovery of atomically thin structures with a high density of coordinatively unsaturated metal sites (CUMS) and a large electrochemically active surface area. This will enable not only the production of low-cost and mass-efficient large-area metal-based catalysts that is important in terms of rational PGM use, but will also improve the overall catalytic performance towards HERs by utilizing CUMS as catalytically active centers. Indeed, surficial atoms of 2D metal nanosheets have low coordination numbers and, thus, can facilitate hydrogen proton adsorption for the efficient HER. This is because almost all the metal atoms in the 2D catalyst will be involved in the catalytic reaction. Such highly exposed CUMS can eventually increase the utilization efficiency of NMs while maintaining their outstanding catalytic properties. Furthermore, as demonstrated by the specific example of subnanometric Ru clusters,[23] low-coordinated Rh clusters exhibit upshifted d band centres and hence are more catalytically active in the HER compared to highly coordinated Rh structures. A similar effect of the coordination number on the d band centre was also reported for Pt[24] and Au[25] nanoclusters. The above highlights the exceptional importance of 2D metals with an abundance of low-coordinated atoms as promising novel HER catalysts.

This work provides a brief overview of the currently existing approaches and challenges in the growth of 2D noble metals and summarizes the use of selected 2D metals as catalysts for the hydrogen evolution reaction.

2. Advances in the synthesis of 2D noble metals

Modern HER electrocatalyst design concepts require a more rational utilization of NMs especially PGMs to achieve their catalytic activity, comparable to that of the state-of-the-art commercial Pt/C catalysts. A possible way toward the sustainable use of these precious resources is coordination engineering of NMs that can be efficiently realized through the creation of atomically thin metal catalysts. In this regard, a profound theoretical and experimental comprehension of the fundamental mechanisms behind the formation of low-coordinated 2D NMs is of particular importance. From a theoretical point of view, most two-dimensional metals are predicted to be stable, at least when they have hexagonal and honeycomb structures.[26] This prediction was mainly reached based on an estimation of the cohesive energy and in-plane elastic constants at 0 K. However, the room-temperature stability of 2D metal nanosheets is still an unaddressed issue. Intuitively, one can expect a 2D-to-3D transition for metals possessing a relatively low 0 K-cohesive energy for their 2D structure and a comparatively large 0 K-cohesive energy for their 3D counterpart. According to Fig. 1, close-packed hexagonal 2D metal lattices are energetically less stable than their bulk counterparts. Taking the above into account and considering the connection between cohesive energy and surface energy (the stronger the cohesion, the higher the surface energy), it can be concluded that the growth of 2D noble metals is quite a challenging task due to their strong tendency to agglomerate to
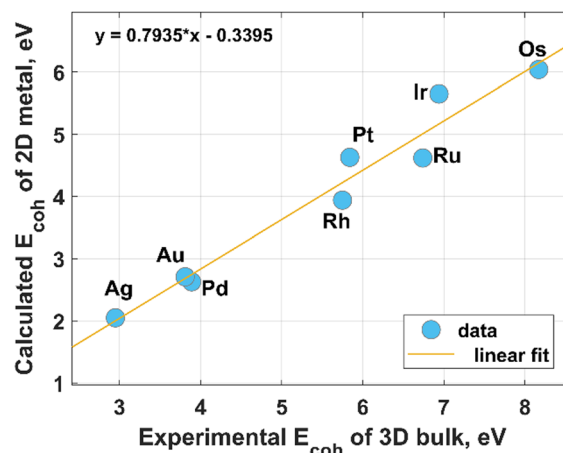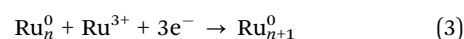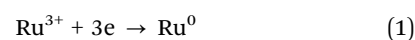

Fig. 1 Relationship between the experimental values of the cohesive energy of bulk noble metals and the theoretically predicted cohesive energies for their 2D counterparts. The experimental data were extracted from the literature,[29] while the theoretical data for hexagonal structures were reported by Nevalaita and Koskinen.[26]

form 3D close-packed structures.[27] In other words, there are inherent thermodynamic restrictions to prevent anisotropic growth of metal nanosheets, which can be, however, eliminated or avoided through realization of the kinetically controlled synthesis. Nevertheless, due to the adaptability and flexibility of conventional physical and chemical methods (like atomic layer deposition, magnetron sputtering, chemical vapor deposition, thermal evaporation, electrodeposition) to meet strict conditions for thin-film deposition at an extreme thickness limit, these techniques are also broadly used for the formation of 2D metals. However, in this case, the need to make an appropriate choice of substrate comes to the forefront. Indeed, the wetting nature of the metal film on the substrate, and hence the film growth regime (2D or 3D), is strongly dependent on the metal-substrate interaction.[28] The possible routes for the synthesis of 2D noble metals are introduced in the following subsections.

2.1. Ruthenium

In their recent study, Chen *et al.*[30] reported the synthesis of two-dimensional ruthenium nanocrystals using an O_2-mediated solution-based colloidal method. More specifically, 2D Ru is formed in three stages, including: (i) the initial reduction of the $RuCl_3$ precursor (at 180 °C) followed by the appearance of small irregularly shaped Ru nanosheets, (ii) a gradual in-plane dendritization and (iii) a final filling of the empty channels between the separated Ru branches by the Ru atoms, respectively (Fig. 2). From a kinetics point of view, the growth process can be understood as an aggregation of freshly reduced zero-valent Ru atoms (Ru^0) towards the formation of early-stage nuclei and enlarged Ru_{n+1}^0 clusters:

$$Ru^{3+} + 3e \rightarrow Ru^0 \tag{1}$$

$$n(Ru^0) \rightarrow Ru_n^0 \tag{2}$$

$$Ru_n^0 + Ru^{3+} + 3e^- \rightarrow Ru_{n+1}^0 \tag{3}$$

8282 | *Phys. Chem. Chem. Phys.*, 2023, **25**, 8281–8292

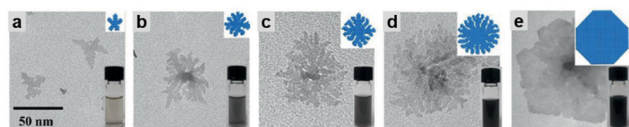This journal is © the Owner Societies 2023

Fig. 2 Time evolution of the morphology of Ru nanosheets. Transmission electron microscopy (TEM) images were made at different reaction times: (a) 180 min, (b) 190 min, (c) 200 min, (d) 220 min, and (e) 420 min. Reproduced with permission from ref. 31. Copyright 2020 Wiley-VCH GmbH.

Fig. 3 An illustration of the transformation of exfoliated RuO_2 nanosheets into a Ru monolayer. Reproduced with permission from ref. 37. Copyright 2013 American Chemical Society.

X-Ray diffraction (XRD) and X-ray photoelectron spectroscopy (XPS) measurements allowed authors to reveal that the free-standing 2D Ru has a hcp structure with a (001) basal plane and is completely metallic (only Ru–Ru bonds were identified). This result allows us to exclude the formation of RuO_2 under synthesis conditions. Indeed, the oxidation requires heat treatment at 300 °C for 1 h under 5% H_2/Ar and air. This is in good agreement with the previous finding, according to which the oxidation of single-crystalline Ru(0001) surfaces begins only above 550 K (or 277 °C).[31] The important role of O_2 gas in decreasing the reduction rate of the Ru^{3+} to 0.10 mM min^{-1} was highlighted, if we compare it with that of the Ar-controlled process (0.43 mM min^{-1}). 4.3-fold slowdown of the Ru^{3+} reduction reaction that entails a limitation of the atom attachment/addition to the growth front is a key factor causing the formation of 2D ruthenium nanosheets. Indeed, the use of stronger reducing agents like H_2 and Ar gave rise to the growth of Ru nanoparticles and Ru nanowires rather than the formation of planar ruthenium nanosheets. This indicates a distinct possibility of forming 2D Ru *via* kinetic control.

A similar solvothermal approach was applied to form Ru nanosheets of ∼1.0–1.2 nm thickness (approximately 5–7 atomic layers) through the reduction of Ru acetylacetonate at 180 °C over 18 h in the presence of urea and isopropanol.[32] It was stated that the isopropanol is responsible for the directional (anisotropic) growth of Ru nanosheets, while the urea can stave off the aggregation of the initially separated Ru nanosheets, thereby promoting the in-plane growth mode.

Several efforts were also made to grow ultrathin Ru films on glass,[33] Au (111)[34] and Si(100)[35] substrates by atomic layer deposition (ALD), electrochemical deposition and dc-magnetron sputtering, respectively. In most cases, the supporting substrate may significantly affect the growth mode and physicochemical properties of the deposited films. However, the mentioned examples concern not only different substrates, but also different growth methods. This brings additional method-related influencing factors on Ru growth. Therefore, a direct comparison between the corresponding growth modes would be incorrect. At the same time, it can be noted that the Ru film on gold is relatively homogeneous.[34] This is due to a small lattice misfit between Au(111) and Ru(0001) that promotes Ru heteroepitaxy on gold surfaces. Meanwhile, Ru film growth on more lattice-mismatched substrates like silicon[35] and glass[33] resulted in the formation of the polycrystalline phase (grained films). The presence of the grain boundaries in polycrystalline film leads to the appearance of unique catalytically active sites that are missing in the continuous layers. This can eventually affect the
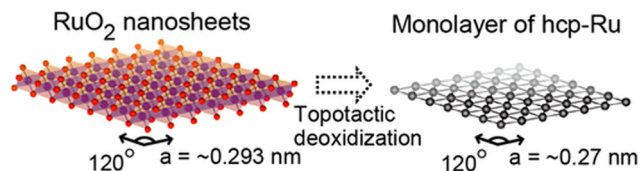
HER performance of Ru catalysts. Furthermore, as was recently demonstrated,[36] the substrate properties may influence the catalytic performance of 2D metal. It was revealed that modulation of the charge transfer at the 2DAu/SiC interface affected the d band center of the gold layer and the Gibbs free energy of hydrogen adsorption (generally accepted descriptors of the HER). The same phenomena can be expected in the case of Ru film. Nevertheless, since in almost all cases the thickness of the resulting Ru films exceeds 2 nm, they cannot be classified as true atomically thin Ru layers. The catalytic properties of such Ru layers may be interesting in their own right.

One more interesting approach for the synthesis of 2D Ru was originally proposed by Fukuda et al.[37] This method called topotactic metallization involves the reduction of pre-synthesized exfoliated RuO_2 nanosheets with subsequent formation of the ruthenium monolayer (an average thickness of ∼0.6 nm) with hexagonal symmetry (Fig. 3). The successful reduction was achieved through treatment in a gas mixture atmosphere (5% H_2 + 95% N_2) at 200 °C. Since Ru is believed to be one of the best catalysts for ammonia synthesis,[38] then the question arises as to whether the use of a (5% H_2 + 95% N_2) gas mixture in the presence of Ru catalyst can cause a NH_3 synthesis reaction. Since the authors in ref. 37 have not commented on the possibility of ammonia production by the conventional Haber–Bosch process, one can assume that the proposed synthesis conditions are far different from those that initiate the reaction using a Ru/C catalyst (T = 460 °C, P = 50–100 bar, H_2/N_2 ratio of 1.5).[39]

2.2. Iridium

From Fig. 1 it is clear that iridium has quite a high value of cohesive energy for the 3D phase that makes the synthesis of atomically thin Ir layers extremely challenging. For this reason, only several studies on the growth of ultrathin Ir layers have been published to date.[40,41] The performance of the wet-chemical method for the synthesis of freestanding ultrathin Ir nanosheets (with a thickness of 5–6 atomic layers) has been explored in ref. 40. This method is based on the thermal decomposition of formic acid into H_2 and CO components at 100 °C for 5 h that is accompanied with a reduction of $IrCl_3$ precursor using released reducing agents (Fig. 4). It was also emphasized that CO plays a dual role of the reducing agent and a surface-confining agent. The latter is a necessary condition for the lateral growth of Ir over the (111) plane. Moreover, partial hydroxylation of the surface was suggested as a possible reason for the minimization of the surface energy and the formation of the stable 2D structure of iridium.

This journal is © the Owner Societies 2023

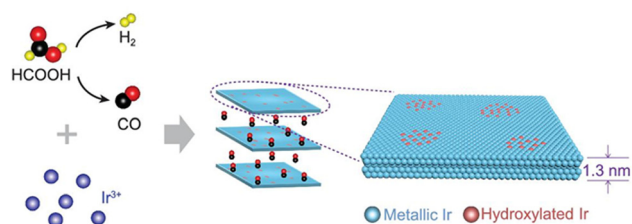*Phys. Chem. Chem. Phys.*, 2023, **25**, 8281–8292 | **8283**

Fig. 4 The proposed mechanism underlying the formation of the Ir nanosheets. Reproduced with permission from ref. 40. Copyright The Author(s) 2020. Published by Oxford University Press on behalf of China Science Publishing & Media Ltd.

These results provide a good scientific background for further experimental work towards obtaining the iridium monolayer.

Attempts to grow the nanometre iridium films onto a porous anodic alumina (PAA) template by using an atomic layer deposition technique have also been reported.[41] However, the measured thickness of 3 nm is pretty far from the true 2D limit. It remains to be seen whether the atomic layer deposition can be used to synthesize a large-area iridium monolayer. Probably, the key to solving this problem lies in the optimization of the reaction chamber and the iridium source temperatures during ALD cycles.

2.3. Rhodium

Belonging to platinum-group metals and possessing superior catalytic activity, Rh in 2D form is of special interest for catalysis due to its internal physical and chemical properties.[42] Like other 2D noble metals, Rh nanosheets are synthesized mainly in the presence of surface-capping agents.[43–45] Polyallylamine hydrochloride (PAH) was used as a capping and shape directing agent to form carbon nanotube (CNT)-supported 2D rhodium nanosheets with a thickness of 0.9 nm[43] and free-standing ultrathin rhodium nanosheet layers with a thickness of 0.8 nm that correspond to 6 atomic layers.[44] In both cases, the mechanism underlying the formation of 2D Rh nanosheets lies in inhibiting the isotropic growth by the attached polyallylamine hydrochloride molecules (Fig. 5A). The strong interaction between PAH and $RhCl_3$ precursor molecules lowers the reduction rate of $RhCl_3$ precursor, enabling kinetically controlled synthesis. The process starts with reducing Rh^{3+} to Rh^0 under heating conditions (at 120 °C) followed by the formation of small Rh nanoparticles with a size of 3 nm after 30 min and their gradual transformation to dendritic Rh nanosheet nanoassemblies over 1.5 h. The points of attachment of capping molecules provide necessary conditions for the appearance of 2D Rh nuclei and eventual formation of atomically thick ultrathin Rh nanosheets. The synthesis time of 6 h was identified as the time frame sufficient enough to form a final product – Rh nanosheet nanoassemblies with a mean size of 95 nm.

Another research study[45] described the growth recipe of single-layered rhodium nanosheets (with a thickness of $\sim$4 Å) that is based on the reduction of $Rh(acac)_3$ at 180 °C for 8 h in the presence of poly(vinylpyrrolidone) (PVP) surfactant. This method enables Rh nanosheets to be obtained with an edge
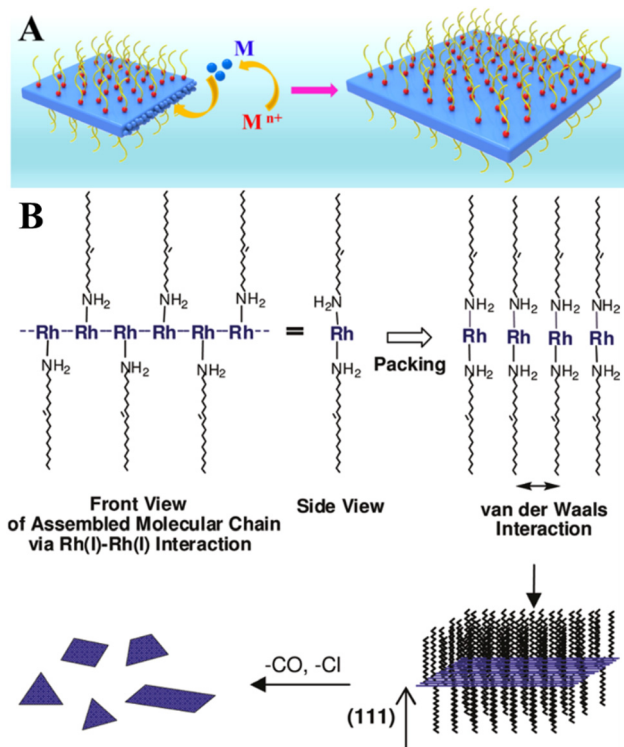

Fig. 5 (A) The illustration of the confinement growth of 2D Rh nanosheets at 120 °C for 6 h. Reproduced with permission from ref. 44. Copyright © 2016 American Chemical Society. (B) A possible growth mechanism of 2D Rh nanoplates proposed by Jang et al.[36] Reproduced with permission from ref. 47. Copyright © 2010 American Chemical Society.

length of approximately 500–600 nm. Despite the efficiency of these methods, it is felt that using of surface-capping agents is in principle undesirable and should be avoided.[46] This is due to the fact that the capping molecules may hinder the chemical reaction between the metal surface and targeted substances (for example, hydrogen protons, water molecules, hydronium ions), thereby adversely affecting the catalytic performance of 2D metal layers especially towards the HER. In this regard, the cyanogel-reduction method proposed by Liu et al.[46] implies the capping agent-free synthesis of ultrathin rhodium nanosheets (3–4 atomic layers) through the reduction of a jelly-like $RhCl_3$–$K_3Co(CN)_6$ cyanogel with formaldehyde at 180 °C for 12 h. It was argued that the 2D structural units of the 3D cyanogel skeleton serve as a self-platform for the formation of 2D Rh nanosheets. In line with this, earlier work by Jang and others[47] showed that extremely thin Rh nanoplates (average thickness of 1.3 $\pm$ 0.2 nm) can be synthesized through the reaction between $[Rh(CO)_2Cl]_2$ precursor and oleylamine. It was hypothesized that the formation mechanism is based on the strong metal-metal interaction between the dissolved Rh precursor molecules. Since the resulting Rh-based complex has a chain structure, the van der Waals interaction between the neighboring chains (via alkyl groups) may result in the formation of a lamellar structure and a gradual self-assembling of reduced Rh^0 species into 2D plates (Fig. 5B).

Another example of the surfactant-free synthesis of the ultrathin Rh layers with thicknesses from 1 to a few monolayers

8284 | *Phys. Chem. Chem. Phys.*, 2023, **25**, 8281–8292

This journal is © the Owner Societies 2023

is a direct layer-by-layer growth of Rh onto single-crystal Ru(0001) by means of an e-beam evaporator.[48] Rh films were grown in an ultrahigh vacuum chamber at a growth temperature of 650 K and a base pressure of 10^{-10} mbar. These conditions enable us to avoid atom intermixing at the Rh/Ru interface and undesired adsorption of residual gases. It was revealed that the first Rh layer grows pseudomorphically, completely reproducing the hcp structure of the Ru substrate. However, the second one and next layers stack in an fcc sequence.

2.4. Osmium

There is practically no information on the existence of osmium in 2D form (having only one monolayer). This is partly due to its highest cohesive energy (for both 2D and 3D cases), as was shown in Fig. 1, and hence a high melting point that makes it impossible to easily grow the Os layers. Other drawbacks limiting the Os-involved experimental studies include its natural scarcity, and its tendency to form highly toxic and volatile OsO_4 tetroxide by reacting with atmospheric oxygen under ambient conditions.[49] Wet chemical synthesis approaches enable the growth of only Os nanoparticles of very small size (<2 nm).[50] This specificity of osmium complicates the formation of large area 2D Os layers by using the kinetically controlled process. Meanwhile, growth by deposition techniques is an appealing alternative to form the continuous Os monolayer *via* using, for example, strongly-interacting substrates. This eventually might lead to good wetting characteristics of the Os film. A systematic review of the existing literature, including reports on the growth of thin osmium films by using a differential potential pulse deposition method,[51] atomic layer deposition,[52] chemical vapor deposition,[53–55] and magnetron sputtering,[56] has highlighted a potential pathway for the synthesis of true 2D Os layers. In particular, a more beneficial combination of the molecular precursors for ALD/CVD growth and supporting substrates could facilitate a template-assisted 2D growth regime of osmium. In this context, a recent report on the modification of graphene by osmium adatoms (up to reaching 18% coverage)[57] indicates that graphene can be potentially used as a substrate for the formation of 2D Os nanopatches (due to the strong tendency of the metal adatoms to form the clusters). Adjusting the osmium-graphene interaction is a promising tool to control the Os cluster planarity and a transition between 2D and 3D cluster shapes. In general, there are different approaches to controlling a metal–graphene interaction. This control can be achieved through defect,[58] strain,[59] and substrate[36] engineering. Moreover, appropriate surface modification of graphene by functional chemical groups also enables fine tuning of the metal–graphene interaction.[60] Although these techniques were initially exploited to alter the strength of the interaction between graphene and other metals than osmium, their scope can be also extended to the Os case.

2.5. Palladium

Probably due to a comparatively low cohesive energy (Fig. 1), palladium is more prone than the previously considered metals to forming extremely thin 2D nanosheets by means of top-down methods. According to earlier reports, successful deposition of

a Pd monolayer onto Al (111),[61] Pt(111),[62] Ni(111),[63] Mo (100),[64,65] Ta (110),[66] Re{0001},[67] and HOPG[68] can be achieved through a thermal evaporation approach. Among the most common methods for the synthesis of 2D Pd layers is CO-mediated growth,[69–73] electrochemical deposition,[74–76] and the reduction of a $PdCl_2$-graphite intercalation compound precursor.[77–80] An unusual route to grow two-dimensional palladium dendritic nanostructures was proposed by Zhu *et al.*[81]

The method is based on *in situ* liquid-cell transmission electron microscopy (TEM). Within this approach, electron beam irradiation of the liquid tetrachloropalladate precursor surrounded by two SiN membranes resulted in the reduction of the palladium ions to Pd^0 followed by the formation of the initial Pd nuclei on SiN and a gradual growth of branched nanostructures by a diffusion-limited aggregation mechanism (Fig. 6).

2.6. Platinum

Due to its outstanding catalytic performance, platinum has received great attention from the research community for a long time. However, the high cost of bulk platinum hinders the large-scale production of Pt-based catalysts and is a trigger for the development of new technologies assuming reduction of the platinum consumption with a simultaneous increase in active surface area. In this context, the implementation of 2D Pt-based technologies is a reliable strategy to meet the above-mentioned challenge.

In earlier works, Madey *et al.*[82] and Schröder *et al.*[83] reported the deposition of atomically thin Pt layers on metallic substrates like W and Cu surfaces by the evaporation technique. It was shown that 2D Pt film growth at room temperature proceeds through layer-by-layer growth rather than by island growth mode (at least for the first two monolayers). The detrimental role of the oxygen atmosphere on the stability of the platinum monolayer was underlined.[82]
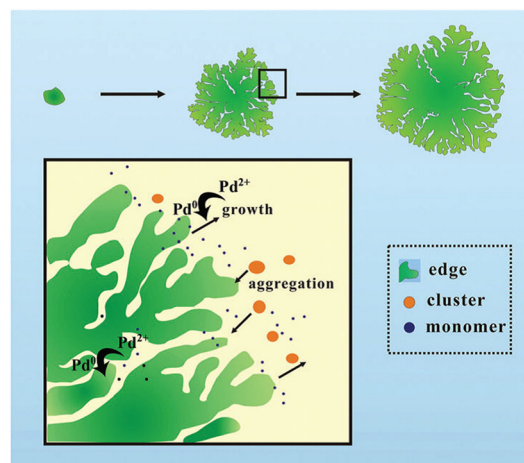

Fig. 6 A sketch of the mechanism of the formation of the 2D Pd dendritic nanostructures. Reproduced with permission from ref. 81. Copyright © 2014 The Royal Society of Chemistry.

This journal is © the Owner Societies 2023

Phys. Chem. Chem. Phys., 2023, **25**, 8281–8292 | **8285**

As was shown later, the growth of continuous 2D Pt layers on non-metallic substrates (Si(111),[84] TiO$_2$-terminated SrTiO$_3$ (001),[85] SiO$_2$/Si[86]) by different deposition techniques (magnetron sputtering and electron beam evaporation) is quite a challenging task due to their unsuitable wettability. Instead, the formation of Pt nanocluster/nanoisland arrays is usually observed. However, since the height of the Pt islands/clusters is controllable (until reaching 0.13 nm[84]) they are of interest to catalytic applications in their own way. Concomitantly, an ALD technique was found to be the more effective method to forming continuous ultrathin Pt layers on graphene oxide[87] and titanium carbide (TiC),[88] respectively. For example, the use of MeCpPtMe$_3$ as a Pt precursor and ozone as a co-reactant enabled the formation of stable Pt films with thicknesses ranging from 1 to 6 monolayers.[88]

Surface-limited redox replacement (SLRR) is another promising approach to form a Pt bilayer or monolayer on graphene[89] or gold.[90] The core of this method is based on the galvanic displacement on a underpotentially deposited (UPD) Cu layer (sacrificial metal) by the platinum. In contrast, there are a few reports on more economically beneficial galvanic-replacement-free electrochemical deposition of Pt overlayers on Ag nanocrystals[91] and 111 textured Au thin films.[92]

Surfactant-directed solution-phase synthesis was proposed as a facile route to grow two-dimensional ultrathin single-crystalline platinum nanodendrites in aqueous solution under ambient conditions.[93] The formation mechanism implies the initial chemical reaction between C$_{22}$N–COOH (Br$^-$) surfactant that acts as a structure-directing template and facet-capping agent and H$_2$PtCl$_6$ in the presence of ascorbic acid (reducing agent). This reaction is followed by stabilization of the C$_{22}$N–COOH/PtCl$_6$$^{2-}$ lamellar mesophase with subsequent reduction of PtCl$_6$$^{2-}$ into 2D Pt nanocrystals (Fig. 7). Although the thickness of these metal nanodendrites is 2.3 nm, there is ample room for their thinning *via* adjusting the growth conditions.

A carbon-rich $(6\sqrt{3} \times 6\sqrt{3})$ R30° surface reconstruction of SiC also called a buffer layer and zero-layer graphene was recently identified as a promising template for growth of 2D Pt (with a thickness of 3–4 Å) by a physical vapor deposition technique.[94] Due to the fact that approximately 30% of carbon atoms belonging to the buffer layer are covalently bonded to the silicon atoms of the SiC substrate, the buffer layer is corrugated, acting as a unique sp^2–sp^3 hybrid platform that is capable of preventing the formation of 3D Pt islands at early growth stages. This arises from the nonuniform potential energy landscape caused by the presence of sp^3-bonded carbon atoms.

Masayuki Shirai and their colleagues[95,96] proposed that the hydrogen reduction of platinum tetrachloride intercalated between graphite layers can also be used as a possible method for the synthesis of two-dimensional platinum nanosheets (1–3 nm in thickness and 100–500 nm in width) between the graphite layers.

2.7. Gold

According to Fig. 1 the cohesive energy of gold is comparable to that of the Pd. This creates good preconditions for the synthesis of 2D gold nanosheets by using top-down approaches. In particular, two research groups reported the synthesis of free-standing two-dimensional gold membranes using *in situ* transmission electron microscopy.[97,98] One of the approaches suggests the initial welding of two Au nanocrystals followed by the induction of in-plane tensile strain near the grain boundary region.[97] This manipulation resulted in the extreme mechanical thinning of the local Au bicrystal region and a final formation of the free-standing 2D Au membrane (Fig. 8). The resulting atomically thick membrane had a simple-hexagonal lattice. A similar approach was based on *in situ* dealloying of the Au–Ag alloy during the TEM.[98] E-beam exposure of the alloy causes much faster sublimation of the Ag atoms from the exposed region compared to Au atoms. As a result, the remaining gold atoms diffuse to vacancy sites and gradually form a hexagonally close-packed Au monolayer.

Another type of 2D Au synthesis method involves directly depositing extremely thin gold layers on foreign substates, which makes it possible to facilitate the using of 2D Au for catalytic applications through avoiding process steps related to 2D Au transfer to the preferred substrate. In this regard, some efforts have been dedicated to forming 2D Au on C$_{60}$ covered HOPG,[99] defect-free boron nitride nanotubes (BNNTs),[100] Au(111)/HOPG[101] and MgO/Ag(001).[102] However, despite that in all mentioned cases the obtained 2D Au product is atomically thin, it can be referred to the planar islands or even small 2D clusters rather than to large-area monolayers. It is interesting to
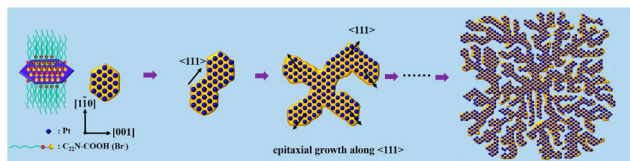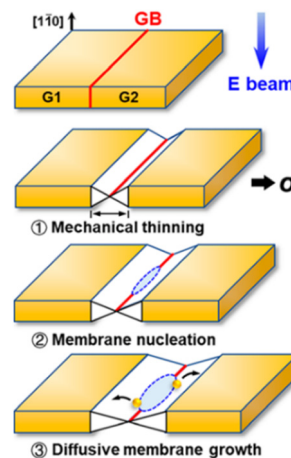

Fig. 7 The mechanism of the step-by-step in-the-plane epitaxial growth of platinum nanodendrites. Reproduced with permission from ref. 93. Copyright © 2019 American Chemical Society.

Fig. 8 A sketch of the mechanical thinning mechanism of the formation of a 2D gold membrane using *in situ* TEM. Reproduced with permission from ref. 97. Copyright © 2020 American Chemical Society.

8286 | *Phys. Chem. Chem. Phys.*, 2023, **25**, 8281–8292

This journal is © the Owner Societies 2023

note that recent progress in the sublimation growth of high-quality and large-area buffer layers on SiC enabled this platform to be exploited to host the gold atoms.[103] More specifically, the annealing of the vapor-deposited gold nanostructures on the buffer layer led to the intercalation of the gold species below the buffer layer, with subsequent conversion of the buffer layer to quasi-free-standing graphene. This enables confining the gold atoms and their self-assembly into a 2D Au layer with semiconducting properties.

Wet chemistry synthesis strategies have also been applied to grow 2D Au nanosheets.[104–107] Jeong et al.[104] used L-arginine as the reductant and the capping agent to reduce hydrogen tetrachloroaurate trihydrate ($HAuCl_4 \cdot 3H_2O$) at 95 °C for 2 h in order to form single-layered Au nanosheets with a mean lateral size of 11.65 μm. Another reported method dealt with the array of uniform 2D gold clusters formed on Si using colloidal solutions in the presence of liquid CO_2.[105] A promising wet chemistry method for the facile synthesis of 2D Au nanosheets (only 1–2 atomic layers) using a layered double hydroxide (LDH) template was proposed by Wang et al.[106] This method involves the reaction between Au precursor ($AuCl_4$) and Mg/Al-LDH that accompanied the insertion of $AuCl_4$ species between layers of LDH and their reduction by using $NaBH_4$ (Fig. 9).

A further example of an aqueous approach is represented by a methyl orange (MO)-mediated synthesis method that exploits aqueous solutions of $HAuCl_4$, $Na_3C_6H5O_7$ and MO to form highly catalytically active 2D Au nanosheets with a thickness of only 0.47 nm under ambient conditions.[107] In this case, methyl orange acts as a confining agent.

2.8. Silver

Historically, the growth of extremely thin silver layers including 2D Ag has been studied over the years. Like other noble metals, vapor-deposited Ag monolayers on different substrates (Ge(111),[108] Ru(001),[109] Si(111),[110] Ni(111),[111] W(110),[112] Ni(001),[113] Cu(001),[114] graphite[115]) were initially in focus. In parallel with this, a set of experiments related to the electrochemical deposition of 2D Ag layers under Langmuir films (negatively charged organic monolayers[116–118] or even neutral amphiphilic Schiff bases[119]) was carried out in the 1990s. In most cases, a 2D growth regime manifests as the formation and evolution of the dendritic silver nanostructures below organic monolayers. It was stressed that the morphology of such nanostructures is defined by a balance between the surface pressure of the Langmuir monolayer, an applied voltage, and a silver ion concentration.

More recent approaches utilize organic or non-organic layered templates (redox-active tyrosine-mediated Peptide[120]

and layered double hydroxide (LDH),[121] for example) to synthesize 2D Ag in the interlayer space by using wet chemistry. In the former case, the key step is the binding of silver ions to the peptide at the cysteine sites. As a result, Ag ion-coordinated peptide monomers interact with each other so that the multilayer stacking in the peptide template is formed at the air/water interface through π–π interactions between aromatic side chains (Fig. 10A). At the final stage, the reduced Ag species located between the peptide layers tend to self-assemble into 2D layers. Although further practical application of synthesized 2D Ag seems to be challenging due to the possibly detrimental effects of the organic template on the electronic properties of the metal nanosheets, the authors in ref. 120 argued that their structures possess excellent electrical properties even without the removal of the organic surfactant.

The use of a hard inorganic LDH template to provide the conditions for anisotropic growth of 2D Ag is another promising approach. This method suggests exploitation of a 2-dimensional silver carboxylthiolate (Ag-3-M-NS) as the precursor (Fig. 10B). It was shown that the layered structure of LDH acts as an effective platform for interlayer confining of the silver carboxylthiolate and its subsequent reduction to Ag^0. It was emphasized that a worthwhile hard inorganic LDH template can be removed via acid treatment while keeping the 2D nature of the silver nanosheets intact.
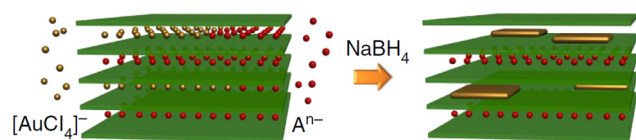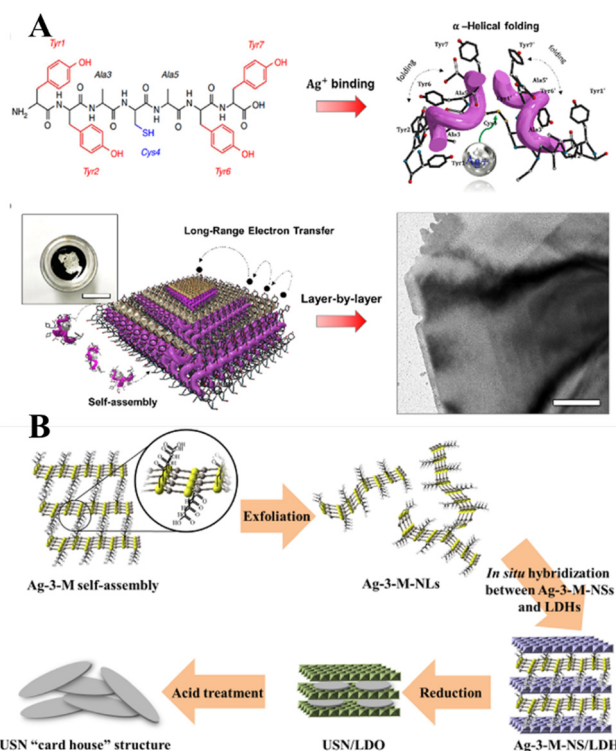

Fig. 10 (A) Schematics of the peptide-template-mediated formation of 2D Ag layers.[120] Reproduced with permission from ref. 120. Copyright © 2020 American Chemical Society. (B) Illustration of the formation process of single Ag layers within the interlayer space of LDH. Reproduced with permission from ref. 121. Copyright © 2019 American Chemical Society.

Fig. 9 A possible growth mechanism of ultra-thin 2D Au nanosheets proposed by Wang et al.[106] Reproduced with permission from ref. 106. Copyright © 2015 Macmillan Publishers Limited.

This journal is © the Owner Societies 2023

Phys. Chem. Chem. Phys., 2023, **25**, 8281–8292 | **8287**
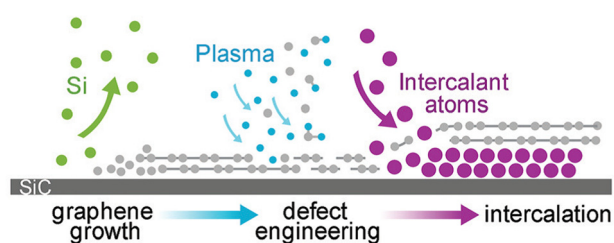
Intercalation Process

Fig. 11 A sketch of the formation of 2D Ag film using epitaxial graphene on SiC as a confining template. Reproduced with permission from ref. 122. Copyright © 2019 The Royal Society of Chemistry.

As was already mentioned, graphenized SiC can be utilized as a host template to accommodate 2D metal layers. In particular, two different cases were considered: (i) the growth of 2D Pt on buffer layer/SiC and (ii) Au intercalation beneath the buffer layer followed by the formation of 2D Au in the space between the decoupled buffer layer and SiC. In contrast, Briggs and colleagues[122] have gone further by utilizing defective monolayer epitaxial graphene on SiC to grow the confined 2D Ag layer. In this regard, the defects provide extra intercalation channels, thereby facilitating the penetration of the evaporated Ag species beneath both the topmost graphene layer and the buffer layer, respectively (Fig. 11).

3. 2D noble metal-based catalysts for the hydrogen evolution reaction

Despite the huge potential of 2D noble metal-based catalysts in the hydrogen evolution reaction, literature analysis has revealed that the HER performance of 2D metals is still relatively understudied. There are only a few experimental studies discussing the benefits of 2D Ru,[30,32] 2D Ir,[40] 2D Rh[43] and 2D Pt[93] as HER electrocatalysts. Chen et al.[30] revealed that among different electrodes including Ru nanowires, Ru nanoparticles and commercial Ru electrodes (Fig. 12A and B), 2D Ru nanosheets synthesized by the O_2-mediated solution-based colloidal method exhibit the most superior HER catalytic activity (with a Tafel slope of 58.6 mV dec^{-1}) under acidic conditions (H_2-saturated 0.1 M $HClO_4$ aqueous solution). This is achieved through favourable combination of electrochemically active specific surface area and Gibbs free energy of the hydrogen adsorption. Improved reaction kinetics arising from the 2D nature of ruthenium was also identified as the main reason of the excellent catalytic properties of 2D Ru formed by a solvothermal approach.[32] Possessing a Tafel slope and overpotential to achieve a current density of 10 mA mg^{-1} that are comparable to those of commercial Pt/C electrodes (46 mV dec^{-1} and 20 mV vs. 31 mV dec^{-1} and 5 mV in in 0.5 M H_2SO_4, respectively), 2D Ru-based electrodes have significant advantages in terms of the metal price, which makes them a nice alternative to platinum (Fig. 12C and D). Based on the analysis of the Tafel slope, it was suggested the Volmer–Heyrovsky mechanism dominates the HER mechanism for 2D Ru. This is in contrast to the Pt electrocatalyst, for which the HER follows the Volmer–Tafel mechanism. For 2D Ru, the rate of the HER was limited by the desorption process.

Switching to other noble metals, it is worth noting that the electrochemical electrodes based on partially hydroxylated 2D iridium nanosheets show an outstanding HER catalytic performance under both acidic (0.5 M H_2SO_4) and alkaline conditions (in 1 M KOH) manifested as the 50 mV-improvement in overpotential (at 10 mA cm^{-2}) compared to commercial Pt/C and Ir/C electrodes (Fig. 12E).[40] Those authors underlined the critically important role of the partial hydroxylation in the reaction
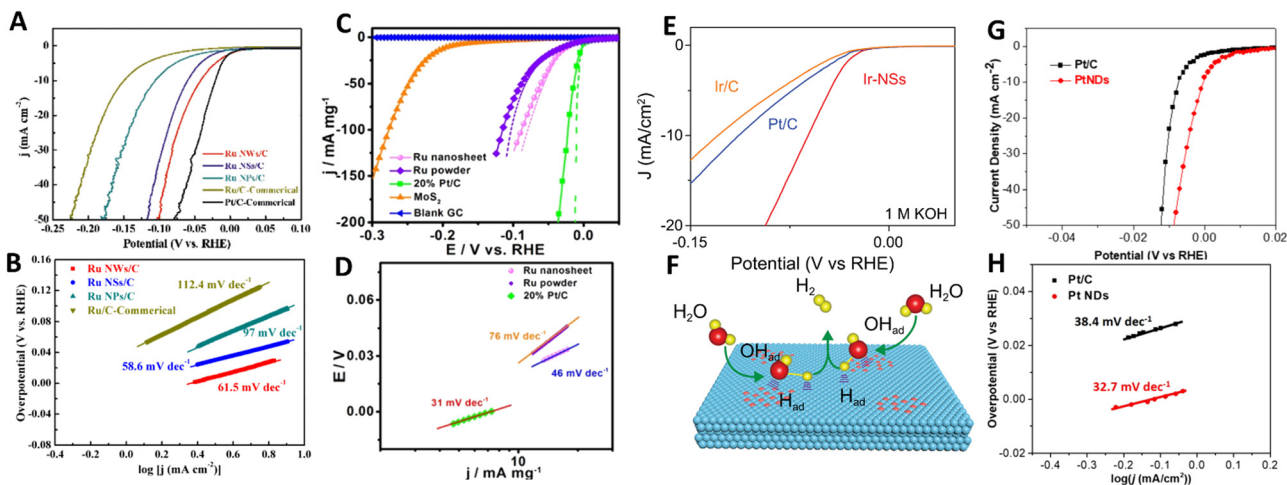

Fig. 12 (A) Linear sweep voltammetry (LSV) curves and (B) Tafel plots of Ru nanosheets for the HER in 0.1 m $HClO_4$ solution. Reproduced with permission from ref. 30. Copyright © 2020 Wiley-VCH GmbH. (C) LSV curves and (D) Tafel plots of Ru nanosheets for the HER in 0.5 M H_2SO_4 electrolyte with pH = 0. Reproduced with permission from ref. 32. Copyright © 2016 American Chemical Society. (E) Polarization curves of Ir nanosheets for the HER in 1 M KOH and (F) an illustration of the HER mechanism for Ir nanosheets. Reproduced with permission from ref. 40. Copyright © Copyright The Author(s) 2020. (G) LSV curves and (H) Tafel Plots of ultrathin Pt nanodendrites. Reproduced with permission from ref. 93. Copyright © 2019 American Chemical Society.

8288 | Phys. Chem. Chem. Phys., 2023, **25**, 8281–8292

This journal is © the Owner Societies 2023

kinetics at the 2D Ir surface. Under acidic conditions H* adsorption mainly occurs at the pristine 2D Ir surface, however, hydroxyl groups on an Ir surface favour H_2O adsorption under alkaline conditions (Fig. 12F). Rhodium is another prominent representative of the catalytically active noble metal groups. Specifically, a unique 2D structure of rhodium nanosheets functionalized by polyallyamine and supported by CNT offers excellent conditions (large electrochemically active specific surface area, good stability, fast electron transport, etc) for the hydrogen evolution reaction in acidic medium (N_2-saturated 0.5 M H_2SO_4).[43] A comparison of the catalytic characteristics of commercial Pt nanocrystals and the synthesized nanosheets is in favor of the latter. In this case, 2D Rh exhibited a lower onset potential compared to that of Pt nanocrystals (−1 mV vs. 10.4 mV, respectively) and a similar Tafel slope (30 mV dec^{-1} vs. 31 mV dec^{-1}). The latter also highlights that the HER at 2D Rh proceeds in a manner similar to that of Pt, with a dominating Tafel reaction mechanism. Two main reasons for the improved HER catalytic activity were singled out: (i) the 2D nature of rhodium nanosheets and (ii) the proton enrichment at the electrode/electrolyte interface due to functionalization of the Rh nanosheets with polyallyamine.

A final example of the 2D-metal-based hydrogen electrocatalyst concerns the platinum that is regarded as a "gold standard" metal for the HER. A transition from bulk Pt to 2D Pt is accompanied by changes in the electrochemical activity towards the HER under acidic conditions.[93] This is mainly caused by an increase in the electrocatalytic active surface area of Pt from 46.4 m^2 g^{-1} for commercial Pt/C to 51.4 m^2 g^{-1} for 2D Pt nanosheets. As a direct consequence of that, 2D Pt demonstrates a smaller overpotential of <0.01 V at a current density of 50 mA cm^{-2} and lower Tafel slope (32.7 mV dec^{-1}) compared to Pt/C, indicating its better electrochemical activity and faster reaction kinetics (Fig. 12G and H). This is however possible not only due to the extraordinary internal properties of 2D Pt, but also due to the presence of the remaining surfactant-related chemical groups at the 2D Pt surface which may alter the hydrogen proton adsorption.

4. Concluding remarks

The current status of research investigations regarding 2D noble metals has been highlighted. Special focus was placed on the synthesis methods and applications of 2D noble metals for the hydrogen evolution reaction. Although the anisotropic growth of 2D metals is a technologically intricate process, which is mainly due to the large surface energy of most metals, a kinetic control approach offers a promising route to synthesize extremely thin 2D metal nanosheets. However, since in most cases the kinetically controlled growth methods require the presence of the surfactant or capping agents the quality of the resulting 2D metal nanosheets suffers from the remaining functional groups on their surfaces that can affect the catalytic performance of 2D metal in unexpected ways. This explains the research efforts to develop surfactant-free and capping agent-free synthesis methods. In line with this, one-step template-assisted

growth of 2D metals by using deposition techniques is of special interest. An appropriate choice of substrate and a fine control of the synthesis conditions (precursor type, temperature, time, pressure etc.) are keys to ensure a 2D growth regime. Although a traditional way to produce metal monolayers implies a pseudomorphic epitaxy on other metal surfaces, more recent approaches include the formation of 2D metals on non-metallic substrates like graphene, graphite, graphenized SiC, etc. The latter one is considered to be a rich platform to host vapor-deposited 2D metal layers atop the surface and to confine them by employing the intercalation process.

2D noble metals are characterized by a high density of coordinatively unsaturated metal sites and large surface area, which make them excellent electrocatalysts for the hydrogen evolution reaction. Even though there are not much experimental data on the catalytic activity of 2D metals towards HERs, the existing results suggest that with appropriate design of selected 2D metals the HER performance can be even better than that of commercial Pt electrodes. This provides both experimentalists and theoreticians with an inspirational framework for further application-focused investigations of 2D metal-based electrocatalysis and more sophisticated design of 2D noble metals.

Conflicts of interest

There are no conflicts to declare.

Acknowledgements

References

1 Hydrogen's growing role in sustainable energy systems, Research*eu, European Commission, 2020, 94, 1-12. https://cordis.europa.eu/article/id/421533-hydrogens-growing-role-in-sustainable-energy-systems.

2 S. van Renssen, Nat. Clim. Chang., 2020, 10, 799–801.

3 Towards Fossil-Free Energy In 2050, European Climate Foundation, 2019.

4 R. Moradi and K. M. Groth, Int. J. Hydrogen Energy, 2019, 44(23), 12254–12269.

5 Y. Huang, Y. Cheng and J. Zhang, Ind. Eng. Chem. Res., 2021, 60(7), 2737–2771.

6 J. Zhu, L. Hu, P. Zhao, L. Yoon Suk Lee and K.-Y. Wong, Chem. Rev., 2020, 120(2), 851–918.

7 M. Ďurovič, J. Hnát and K. Bouzek, J. Power Sources, 2021, 493, 229708.

8 Z. Li, R. Ge, J. Su and L. Chen, Adv. Mater. Interfaces, 2020, 7, 2000396.

9 S. Bai, M. Yang, J. Jiang, X. He, J. Zou, Z. Xiong, G. Liao and S. Liu, npj 2D Mater Appl., 2021, 5, 78.

This journal is © the Owner Societies 2023

Phys. Chem. Chem. Phys., 2023, **25**, 8281–8292 | **8289**

10 J. Zheng, X. Sun, C. Qiu, Y. Yan, Z. Yao, S. Deng, X. Zhong, G. Zhuang, Z. Wei and J. Wang, *J. Phys. Chem. C*, 2020, **124**(25), 13695–13705.

11 S. Wang, A. Lu and C. J. Zhong, *Nano Convergence*, 2021, **8**, 4.

12 C. C. L. McCrory, S. Jung, I. M. Ferrer, S. M. Chatman, J. C. Peters and T. F. Jaramillo, *J. Am. Chem. Soc.*, 2015, **137**(13), 4347–4357.

13 T. Mallouk, *Nat. Chem.*, 2013, **5**, 362–363.

14 C. Li and J.-B. Baek, *ACS Omega*, 2020, **5**(1), 31–40.

15 J. K. Nørskov, T. Bligaard, A. Logadottir, J. R. Kitchin, J. G. Chen, S. Pandelov and U. Stimming, *J. Electrochem. Soc.*, 2005, **152**(2), J23–J26.

16 Communication from the Commission to the European Parliament, The Council, the European Economic and Social Committee and the Committee of the Regions – Critical Raw Materials Resilience: Charting a Path towards Greater Security and Sustainability, 2020.

17 L. M. Salonen, D. Y. Petrovykh and Yu. V. Kolen'ko, *Mater. Today Sustainability*, 2021, **11–12**, 100060.

18 S. Zhang, X. Zhang, Y. Rui, R. Wang and X. Li, *Green Energy Environ.*, 2021, **6**(4), 458–478.

19 M. Datt Bhatt and J. Yong Lee, *Energy Fuels*, 2020, **34**(6), 6634–6695.

20 Y. Chen, K. Yang, B. Jiang, J. Li, M. Zeng and L. Fu, *J. Mater. Chem. A*, 2017, **5**, 8187–8208.

21 W. Moschkowitsch, O. Lori and L. Elbaz, *ACS Catal.*, 2022, **12**(2), 1082–1089.

22 S. Zhang, X. Zhang, Y. Rui, R. Wang and X. Li, *Green Energy Environ.*, 2021, **6**(4), 458–478.

23 Q. Hu, K. Gao, X. Wang, H. Zheng, J. Cao, L. Mi, Q. Huo, H. Yang, J. Liu and C. He, *Nat. Commun.*, 2022, **13**, 3958.

24 E. Toyoda, R. Jinnouchi, T. Hatanaka, Y. Morimoto, K. Mitsuhara, A. Visikovskiy and Y. Kido, *J. Phys. Chem. C*, 2011, **115**(43), 21236–21240.

25 A. Visikovskiy, H. Matsumoto, K. Mitsuhara, T. Nakada, T. Akita and Y. Kido, *Phys. Rev. B: Condens. Matter Mater. Phys.*, 2011, **83**, 165428.

26 J. Nevalaita and P. Koskinen, *Phys. Rev. B: Condens. Matter Mater. Phys.*, 2018, **97**, 035411.

27 Y. Chen, Z. Fan, Z. Zhang, W. Niu, C. Li, N. Yang, B. Chen and H. Zhang, *Chem. Rev.*, 2018, **118**, 6409–6455.

28 D. Bonn, J. Eggers, J. Indekeu, J. Meunier and E. Rolley, *Rev. Mod. Phys.*, 2009, **81**, 739.

29 C. Kittel, *Introduction to Solid State Physics*, John Wiley & Sons, Inc., Hoboken, NJ, 8th edn, 2005, p. 50.

30 Y. B. He, M. Knapp, E. Lundgren and H. Over, *J. Phys. Chem. B*, 2005, **109**, 21825.

31 L. Chen, Y. Li and X. Liang, *Adv. Funct. Mater.*, 2021, **31**, 2007344.

32 X. Kong, K. Xu, C. Zhang, J. Dai, S. N. Oliaee, L. Li, X. Zeng, C. Wu and Z. Peng, *ACS Catal.*, 2016, **6**, 1487–1492.

33 K. Gregorczyk, P. Banerjee and G. W. Rubloff, *Mater. Lett.*, 2012, **73**, 43–46.

34 O. Mann, W. Freyland, O. Raz and Y. Ein-Eli, *Chem. Phys. Lett.*, 2008, **460**, 178–181.

35 Y. B. He, A. Goriachko, C. Korte, A. Farkas, G. Mellau, P. Dudin, L. Gregoratti, A. Barinov, M. Kiskinova, A. Stierle, N. Kasper, S. Bajt and H. Over, *J. Phys. Chem. C*, 2007, **111**, 10988–10992.

36 I. Shtepliuk and R. Yakimova, *RSC Adv.*, 2023, **13**, 1125–1136.

37 K. Fukuda, J. Sato, T. Saida, W. Sugimoto, Y. Ebina, T. Shibata, M. Osada and T. Sasaki, *Inorg. Chem.*, 2013, **52**, 2280–2282.

38 N. Saadatjou, A. Jafari and S. Sahebdelfar, *Chem. Eng. Commun.*, 2015, **202**(4), 420–448.

39 I. Rossetti, N. Pernicone, F. Ferrero and L. Forni, *Ind. Eng. Chem. Res.*, 2006, **45**(12), 4150–4155.

40 Z. Cheng, B. Huang, Y. Pi, L. Li, Q. Shao and X. Huang, *Natl. Sci. Rev.*, 2020, **7**, 1340–1348.

41 B. Fang, C. Yang, C. Pang, W. Shen, X. Zhang, Y. Zhang, W. Yuan and X. Liu, *Appl. Phys. Lett.*, 2017, **110**, 141103.

42 J. Yin, J. Wang, Y. Ma, J. Yu, J. Zhou and Z. Fan, *ACS Materials Lett.*, 2021, **3**, 121–133.

43 J. Bai, S.-H. Xing, Y.-Y. Zhu, J.-X. Jiang, J.-H. Zeng, Y. Chen and J. Power, *Sources*, 2018, **385**, 32–38.

44 J. Bai, G.-R. Xu, S.-H. Xing, J.-H. Zeng, J.-X. Jiang and Y. Chen, *ACS Appl. Mater. Interfaces*, 2016, **8**, 33635–33641.

45 H. Duan, N. Yan, R. Yu, C.-R. Chang, G. Zhou, H.-S. Hu, H. Rong, Z. Niu, J. Mao, H. Asakura, T. Tanaka, P. J. Dyson, J. Li and Y. Li, *Nat. Commun.*, 2014, **5**, 3093.

46 H.-M. Liu, S.-H. Han, Y. Zhao, Y.-Y. Zhu, X.-L. Tian, J.-H. Zeng, J.-X. Jiang, B. Y. Xia and Y. Chen, *J. Mater. Chem. A*, 2018, **6**, 3211.

47 K. Jang, H. J. Kim and S. Uk Son, *Chem. Mater.*, 2010, **22**(4), 1273–1275.

48 Y. He, A. P. Seitsonen and H. Over, *J. Chem. Phys.*, 2006, **124**, 034706.

49 C. E. Housecroft and A. G. Sharpe, *Inorganic Chemistry*, Prentice Hall, 2nd edn, 2004, 710, 671–673.

50 J. Quinson, *Open Research Europe*, 2022, **2**, 39.

51 A. Ignaszak and E. Gyenge, *Electrochim. Acta*, 2013, **95**, 268–274.

52 J. Hämäläinen, T. Sajavaara, E. Puukilainen, M. Ritala and M. Leskelä, *Chem. Mater.*, 2012, **24**(1), 55–60.

53 Y. Chi, H.-L. Yu, W.-L. Ching, C.-S. Liu, Y.-L. Chen, T.-Y. Chou, S.-M. Peng and G.-H. Lee, *J. Mater. Chem.*, 2002, **12**, 1363–1369.

54 Y. Senzaki, W. L. Gladfelter and F. B. McCormick, *Chem. Mater.*, 1993, **5**(12), 1715–1721.

55 C. Li, W. K. Leong and K. P. Loh, *Appl. Organometal. Chem.*, 2009, **23**(5), 196–199.

56 S. L. Li, C. Y. Ma, Q. Y. Zhang, X. P. Liu, C. Zhang and Z. Yi, *Surf. Coat. Technol.*, 2015, **282**, 1–5.

57 J. A. Elias and E. A. Henriksen, *Ann. Phys.*, 2020, **532**, 1900294.

58 I. Shtepliuk and R. Yakimova, *Phys. Chem. Chem. Phys.*, 2018, **20**, 21528–21543.

59 W. Gong, W. Zhang, C. Ren, X. Ke, S. Wang, P. Huai, W. Zhang and Z. Zhu, *Appl. Phys. Lett.*, 2013, **103**, 143107.

60 S. M. Elgengehi, S. El-Taher, M. A. A. Ibrahim, J. K. Desmarais and K. E. El-Kelany, *Appl. Surf. Sci.*, 2020, **507**, 145038.

8290 | *Phys. Chem. Chem. Phys.*, 2023, **25**, 8281–8292

This journal is © the Owner Societies 2023

61 B. Prick and K. Jacobi, *Phys. Rev. B: Condens. Matter Mater. Phys.*, 1988, **37**, 4408.

62 M. Han, P. Mrozek and A. Wieckowski, *Phys. Rev. B: Condens. Matter Mater. Phys.*, 1993, **48**, 8329.

63 S. Terada, T. Yokoyama, N. Saito, Y. Okamoto and T. Ohta, *Surf. Sci.*, 1999, **433–435**, 657–660.

64 J. M. Heitzinger, S. C. Gebhard and B. E. Koel, *Surf. Sci.*, 1992, **275**, 209–222.

65 J. M. Heitzinger, S. C. Gebhard, D. H. Parker and B. E. Koel, *Surf. Sci.*, 1992, **260**, 151–162.

66 A. Sellidj and B. E. Koel, *Surf. Sci.*, 1993, **284**, 139–153.

67 H. A. Etman, Z. V. Zheleva, G. Held and R. A. Bennett, *J. Phys. Chem. C*, 2011, **115**, 4191–4199.

68 E. De Biasi, A. de Siervo, F. Garcia, F. Vicentin, R. Landers and M. Knobel, *J. Electron Spectrosc. Relat. Phenom.*, 2007, **156–158**, 332–335.

69 M. Z. Yazdan-Abad, M. Noroozifar and N. Alfi, *J. Colloid Interface Sci.*, 2018, **532**, 485–490.

70 C. He, J. Tao and P. Kang Shen, *ACS Catal.*, 2018, **8**, 910–919.

71 X. Yin, X. Liu, Y.-T. Pan, K. A. Walsh and H. Yang, *Nano Lett.*, 2014, **14**, 7188–7194.

72 H. Li, G. Chen, H. Yang, X. Wang, J. Liang, P. Liu, M. Chen and N. Zheng, *Angew. Chem., Int. Ed.*, 2013, **52**, 8368–8372.

73 P. F. Siril, L. Ramos, P. Beaunier, P. Archirel, A. Etcheberry and H. Remita, *Chem. Mater.*, 2009, **21**, 5170–5175.

74 A. Gil, A. Clotet, J. M. Ricart, F. Illas, B. Álvarez, A. Rodes and J. Miguel Feliu, *J. Phys. Chem. B*, 2001, **105**(30), 7263–7271.

75 Y. Su, E. Prestat, C. Hu, V. K. Puthiyapura, M. Neek-Amal, H. Xiao, K. Huang, V. G. Kravets, S. J. Haigh, C. Hardacre, F. M. Peeters and R. R. Nair, *Nano Lett.*, 2019, **19**, 4678–4683.

76 C. Lebouin, Y. S. Olivier, E. Sibert, P. Millet, M. Maret and R. Faure, *J. Electroanal. Chem.*, 2009, **626**, 59–65.

77 J. Walter and H. Shioyama, *Phys. Lett. A*, 1999, **254**(1–2), 65–71.

78 J. Walter, *Philos. Mag. Lett.*, 2000, **80**(4), 257–262.

79 J. Walter, J. Heiermann, G. Dyker, S. Hara and H. Shioyama, *J. Catal.*, 2000, **189**(2), 449–455.

80 D. Mendoza, F. Morales, R. Escudero and J. Walter, *J. Phys.: Condens. Matter*, 1999, **11**, L317.

81 G. Zhu, Y. Jiang, F. Lin, H. Zhang, C. Jin, J. Yuan, D. Yang and Z. Zhang, *Chem. Commun.*, 2014, **50**, 9447.

82 T. E. Madey, K.-J. Song, C.-Z. Dong and R. A. Demmin, *Surf. Sci.*, 1991, **247**(2–3), 175–187.

83 U. Schröder, R. Linke, J.-H. Boo and K. Wandelt, *Surf. Sci.*, 1996, **357–358**, 873–878.

84 H. Yasumatsu, T. Hayakawa, S. Koizumi and T. Kondowa, *J. Chem. Phys.*, 2005, **123**, 124709.

85 W. Guo, A. B. Posadas and A. A. Demkov, *J. Vac. Sci. Technol., B*, 2017, **35**, 061203.

86 R. N. Esfahani, G. Jordan Maclay and G. W. Zajac, *Thin Solid Films*, 1992, **219**(257–265), 257.

87 B. Karasulu, R. H. J. Vervuurt, W. M. M. Kessels and A. A. Bol, *Nanoscale*, 2016, **8**, 19829–19845.

88 D. Göhl, H. Rueß, S. Schlicht, A. Vogel, M. Rohwerder, K. J. J. Mayrhofer, J. Bachmann, Y. Román-Leshkov, J. M. Schneider and M. Ledendecker, *ChemElectroChem*, 2020, **7**, 2404.

89 A. W. Robertson, G.-D. Lee, S. Lee, P. Buntin, M. Drexler, A. A. Abdelhafiz, E. Yoon, J. H. Warner and F. M. Alamgir, *ACS Nano*, 2019, **13**, 12162–12170.

90 M. Hakamada, S. Sakakibara, N. Miyazawa, S. Deguchi and M. Mabuchi, *Sci. Rep.*, 2020, **10**, 9594.

91 H. Liu, P. Zhong, K. Liu, L. Han, H. Zheng, Y. Yin and C. Gao, *Chem. Sci.*, 2018, **9**, 398.

92 S. H. Ahn, Y. Liu and T. P. Moffat, *ACS Catal.*, 2015, **5**, 2124–2136.

93 D. Xu, H. Lv, H. Jin, Y. Liu, Y. Ma, M. Han, J. Bao and B. Liu, *J. Phys. Chem. Lett.*, 2019, **10**, 663–671.

94 K. Ho Kim, H. He, M. Rodner, R. Yakimova, K. Larsson, M. Piantek, D. Serrate, A. Zakharov, S. Kubatkin, J. Eriksson and S. Lara-Avila, *Adv. Mater. Interfaces*, 2020, **7**, 1902104.

95 M. Shirai, *Chem. Rec.*, 2019, **19**, 1263–1271.

96 M. Shirai, K. Kubo, M. Sodeno and H. Nanao, *Chem. – Asian J.*, 2021, **16**, 2035–2040.

97 Q. Zhu, Y. Hong, G. Cao, Y. Zhang, X. Zhang, K. Du, Z. Zhang, T. Zhu and J. Wang, *ACS Nano*, 2020, **14**, 17091–17099.

98 X. Wang, C. Wang, C. Chen, H. Duan and K. Du, *Nano Lett.*, 2019, **19**, 4560–4566.

99 L. Guo, Y. Wang, D.-L. Bao, H.-H. Jia, Z. Wang, S. Du and Q. Guo, *Nanoscale*, 2020, **12**, 21657.

100 S. Bhandari, B. Hao, K. Waters, C. H. Lee, J.-C. Idrobo, D. Zhang, R. Pandey and Y. K. Yap, *ACS Nano*, 2019, **13**, 4347–4353.

101 M. R. Fard and Q. Guo, *J. Phys. Chem. C*, 2018, **122**, 7801–7805.

102 C. Stiehler, Y. Pan, W.-D. Schneider, P. Koskinen, H. Häkkinen, N. Nilius and H.-J. Freund, *Phys. Rev. B: Condens. Matter Mater. Phys.*, 2013, **88**, 115415.

103 S. Forti, S. Link, A. Stöhr, Y. Niu, A. A. Zakharov, C. Coletti and U. Starke, *Nat. Commun.*, 2020, **11**, 2236.

104 E. J. Jeong, E. Im, D. C. Hyun, J. W. Leed and G. D. Moon, *J. Ind. Eng. Chem.*, 2020, **89**, 204–211.

105 J. S. Wang, C. M. Wai, G. J. Brown and S. D. Apt, *Langmuir*, 2016, **32**, 4635–4642.

106 L. Wang, Y. Zhu, J.-Q. Wang, F. Liu, J. Huang, X. Meng, J.-M. Basset, Y. Han and F.-S. Xiao, *Nat. Commun.*, 2015, **6**, 6957.

107 S. Ye, A. P. Brown, A. C. Stammers, N. H. Thomson, J. Wen, L. Roach, R. J. Bushby, P. L. Coletta, K. Critchley, S. D. Connell, A. F. Markham, R. Brydson and S. D. Evans, *Adv. Sci.*, 2019, **6**, 1900911.

108 G. Le Lay, R. L. Johnson, R. Seemann, F. Grey, R. Feidenhans'l and M. Nielsen, *Surf. Sci.*, 1993, **287–288**(1), 539–544.

109 K. Wandelt, K. Markert, P. Dolle, A. Jabłonski and J. J. Niemantsverdriet, *Surf. Sci. Lett.*, 1987, **189–190**, A396.

110 K. Spiegel, *Surf. Sci.*, 1967, **7**(2), 125–142.

This journal is © the Owner Societies 2023

Phys. Chem. Chem. Phys., 2023, **25**, 8281–8292 | 8291

111 S. Mróz, Z. Jankowski and M. Nowicki, *Surf. Sci.*, 2000, **454–456**, 702–706.

112 A. Elbe, G. Meister and A. Goldmann, *Surf. Sci.*, 1998, **397**, 346–353.

113 S. Mróz and Z. Jankowski, *Surf. Sci.*, 1996, **349**, 111–118.

114 M. Nowicki and S. Mróz, *Vacuum*, 1996, **47**(5), 445–449.

115 F. Patthey and W.-D. Schneider, *Surf. Sci.*, 1995, **334**, L715–L718.

116 S. Ravaine, C. Breton, C. Mingotaud and F. Argoul, *Mater. Sci. Eng., C*, 1999, **8–9**, 437–444.

117 G. P. Luo, Z. M. Ai, Z. H. Lu and Y. Wei, *Phys. Rev. E*, 1994, **50**, 409.

118 G. Luo, Z. Al and Y. We, *Chin. Phys. Lett.*, 1994, **11**, 6341.

119 Z. Tai, G. Zhang and X. Qian, *Langmuir*, 1993, **9**, 1601–1603.

120 H. Lee, H.-S. Jang, D.-H. Cho, J. Lee, B. Seong, G. Kang, Y.-S. Park, K. T. Nam, Y.-S. Lee and D. Byun, *ACS Nano*, 2020, **14**, 1738–1744.

121 G.-H. Gwak, M.-K. Kim, W.-J. Lee, D.-G. Jeung, J. Kuen Park, S.-M. Paek and J.-M. Oh, *Inorg. Chem.*, 2020, **59**, 2163–2170.

122 N. Briggs, Z. M. Gebeyehu, A. Vera, T. Zhao, K. Wang, A. De La Fuente Duran, B. Bersch, T. Bowen, K. L. Knappenberger, Jr. and J. A. Robinson, *Nanoscale*, 2019, **11**, 15440.

8292 | *Phys. Chem. Chem. Phys.*, 2023, **25**, 8281–8292

This journal is © the Owner Societies 2023